Simulating Potential Impacts of Climate Change on Sediment Production and Shallow Landslide in Western Japan

APIP, Kaoru TAKARA, Kenichiro KOBAYASHI[1], Yosuke YAMASHIKI, and Eiichi NAKAKITA

(1) GCOE-ARS, CPIER, Kyoto University

Synopsis

This study uses a continuous simulation model to assess the potential implications of climate changes on soil production and slope instability at regional scale in the western part of Japan.   Using the product of a very high-resolution atmospheric global climate model having 20-km spatial resolution (MRI-AGCM20) as the climate forcing data, a calibrated geohydrologic model was implemented with hourly output and 1-km grid resolution.   The results suggest that the river basins hydrological responses to precipitation changes under the future climate is going to have direct impact on soil productions and slope instability. In the future climate condition, peak time and magnitude of gross precipitation in June and July decreases, while it is going to be shifted to and increase in August. The study found a 5-75% increase in August precipitation to be associated with up to an approximate 1% to 20% of change in streamflow discharge, 1% to 30% of increase in soil production and 1% to 50% of increase in shallow landslide probability. Hotspots of significant changes differ according to the time and location.

Keywords: geohydrologic model, climate change, west japan, soil erosion and sediment, shallow landslide.

1. Introduction

Based to the Fourth Assessment Report (AR4) of Intergovernmental Panel of Climate Change (IPCC), global average surface temperature, precipitation and extreme events such as heavy precipitation and droughts have changed significantly, and the changes are very likely to continue (IPCC, 2007). Those changes will very likely increase rainfall-runoff, soil erosion, sediment transportation, landsliding, ecological damage and related environmental. Though some general conclusions about climate change and their impacts have been drawn, especially at macro-scales, the potential damages of climate change in particular regions or farms need to be assessed under specific site conditions. Such information is useful for making decisions on how to adapt management practices to mitigate the adverse impacts of climate change.

Climate changes may cause serious water-related problems in the future, however, the influence of those changes in sediment-related issues

in river basins has not been widely investigated. Climate change also influences the timing and magnitude of runoff and sediment production. There might be changes in rainfall erosivity, hydrologic processes, sediment transport capacity, and indirectly on the soil erodibility through changes in land cover and management.

Different approaches have been developed to assess the impacts of climate change on hydrological responses, soil erosion, sediment yield, and landslides such as long-term temporal or spatial analogues and modeling (Ghosh and Mishra, 2010). Top soil detachment and shallow landslide induced by rainfall and runoff are common hydrological processes in hilly and mountainous areas of western Japan. Since soil moisture is a key parameter for controlling those processes, it was therefore hypothesized that using an integrated physically-based distributed soil erosion, sediment transportation, and landslide model which would share basic hydrology would result in improved prediction of soil erosion and landslides.

This study uses a continuous simulation model to assess the potential implications of climate changes on soil production and slope instability at regional scale in the western part of Japan. The specific objectives are: (1) to investigate and analyze the near future and future climate changes of western Japan; (2) to simulate the potential impacts of climate change on the spatiotemporal dynamics of runoff, soil erosion, sediment transportation and slope instability; and (3) to detect the hotspots of soil production and unstable slope probability changes. The study implemented a new developed grid-cell based distributed geohydrologic model that represents the following water and soil interaction: soil moisture accounting, runoff process generation, surface soil detachments, sediment transportation, slope instability, and dam functions to control floods and sediment discharge.

2. GeoHydrologic Model

A one dimensional physically based distributed hydrological model based on grid-cell kinematic wave rainfall-runoff model (Kojima and Takara, 2003) was developed for simulating hydrological responses and soil saturation. In this modelling framework, catchment topography is represented based on digital elevation model (DEM) which is divided into an orthogonal matrix of square grid-cells. A square area on a node point of a DEM is considered as a sub-catchment, which is called a grid-cell. The river catchment is modeled as a network of grid-cell. Each grid-cell receives flows from upper grid-cells and rainfall on it. These grid-cells are connected to each other with a drainage path defined by the steepest of eight-direction. Discharge and water depth diffuse to the next grid-cell according to predefined eight-direction flow map and routine order determined in accordance with DEM and river channel network data. The hillslopes flow routed and given to the river flow routing model; then the river flow is routed to the outlet.

The model simulates three lateral flow mechanisms including (1) subsurface flow through capillary pore (unsaturated flow), (2) subsurface flow through non-capillary pore (saturated flow) and (3) surface flow on the soil layer (overland flow). At each grid-cell, when the water depth is lower than the equivalent water depth d_m for the maximum volumetric water content in the unsaturated flow θ_m ($d_m = h*\theta_m$), flow is simulated by Darcy law with degree of saturation, $(h_w/d_m)^\beta$, and an unsaturated hydraulic conductivity k_m. If the water depth exceeds the equivalent depth for unsaturated flow, the exceeded water flows as saturated subsurface flow that is simulated by Darcy law with saturated hydraulic conductivity k_a. Once the water depth is greater than the soil layer h times effective porosity θ_a ($d_a = h*\theta_a$), the water flows as surface flow, which is simulated by the Manning's equation. Herein, the basic assumption that the flow lines are parallel to the slope and the hydraulic gradient is equal to the slope. In addition, the kinematic wave

model assumes that rainfall intensity always lower than infiltration rate capacity. Thus it does not consider the vertical water flow, the input rainfall data is directly added to subsurface flow or surface flow according to the water depth on the area where the rainfall dropped. Regarding this mechanism, overland flow happens if the depth of water exceeds the soil water capacity. Details on the derivation of this model equations are given by Sayama and McDonnel (2009).

These processes are represented with a kinematic wave model using function for the stage-discharge relationship. An advantage of the model is that the stage-discharge relationship of each grid-cell reflects the topographic and physical characteristics (i.e., land use and soil type) of its own grid. These three flow processes are represented by the following single set of stage-discharge relationship (Tachikawa *et al.* 2004):

$$q = \begin{cases} v_m d_m (h_w / d_m)^{\beta}, & o \le h_w \le d_m \\ v_m d_m + v_a (h_w - d_m), & d_m < h_w \le d_a \\ v_m d_m + v_a (h_w - d_m) + \alpha (h_w - d_a)^k, & d_a < h_w \end{cases}$$

(1)

$$v_m = k_m i, \ v_a = k_a i, \ k_m = k_a / \beta, \ \alpha = \sqrt{i} / n,$$

where q is discharge per unit width, h_w is water depth, i is the topography gradient, k_m is the saturated hydraulic conductivity of the capillary soil layer, k_a is the hydraulic conductivity of the non-capillary soil layer, d_m is the depth of the capillary soil layer, d_a represents the depths of the capillary and non-capillary soil layers, β is the exponent constant of unsaturated flow (= 2), v_m and v_a are the flow velocities of unsaturated and saturated subsurface flows, respectively, n is the Manning's roughness coefficient varies as a function of land use type, and k is a constant (= 5/3).

Simulation of soil transport processes was also included in the above runoff model. Soil detachment processes associated with inter-rill and rill erosion are implicitly simulated as raindrop splash and surface flow detachment, respectively. The empirical equation of soil detachment by raindrops dr is given

as:

$$d_r = \mu \, k \, k_e = \mu \, k \, 56.48 \, r \,, \qquad (2)$$

where μ is the soil erodibility; k is a parameter; and ke is the total kinetic energy of the raindrops. The concept of sediment transport capacity was used to determine soil detachment or deposition by surface flow d_f (Foster, 1982):

$$d_f = \alpha \, (T_c - c) h_{ws} \,, \qquad (3)$$

where α is a proportionality coefficient; h_{ws} is the surface flow depth; c is the sediment concentration; and T_c is the maximum sediment concentration transport capacity, which determines soil erosion (when $T_c > c$) or deposition (when $T_c < c$). In the present work, the sediment transport capacity was calculated based on Unit Stream Power (USP) theory.

The slope stability model is developed based on the concept of the infinite slope model, using the factor of safety (FS) that considers a failure surface. The following are assumed: (i) failure is the result of translation sliding, (ii) the failure plane and water table are parallel to the ground surface, (iii) failure occurs as a single layer, (iv) the failure plane is of infinite length, and (v) the impacts of adjacent factors are not taken into account. For hillslopes, the safety factor generally is represented as the ratio of the available resisting force (shear strength) to the driving force (shear stress). Instability occurs when the shear strength of a soil layer becomes smaller than the shear stress acting on the soil. The governing equation of the safety factor used in this study is based on a Mohr–Coulomb failure law.
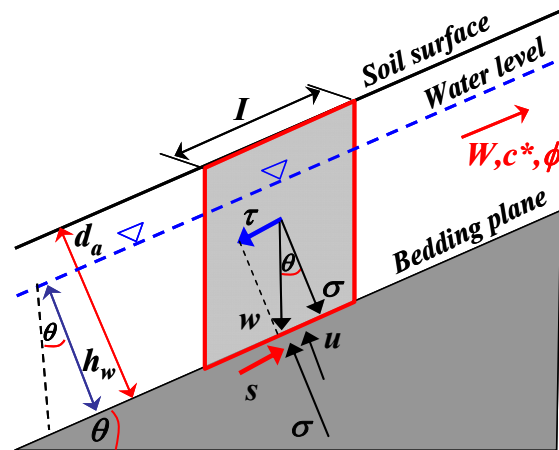
Fig. 1 Forces diagram on a slice of an infinite slope.

Figure 1 illustrates the forces acting on a point along a slope with potential for failure. The resisting force of a soil layer is the shear strength (s) as a combination of forces, including the normal stress (σ), pore pressure (u) within the soil material, cohesion factors (c), and the effective angle of internal friction in degrees (ϕ). The resultant force between normal stress and pore pressure is the effective normal stress. Shear strength based on the Mohr–Coulomb law can be expressed as follows:

$$s = c + (\sigma - u)\tan\phi \qquad (4)$$

Normal stress is the vertical component of gravity that resists downslope movement as follows:

$$\sigma = \rho_s g \cos\theta\, d_a + W\cos\theta , \qquad (5)$$

where ρ_s is the wet soil density (kg/m^3), g is the gravitational acceleration (= 9.81 m/s^2), d_a is the vertical soil depth perpendicular to the slope (m), W is the vegetation surcharge (N/m^2), and θ is the slope angle (deg). Soil moisture increases the unit weight of soil material; therefore it increases both the resisting and driving forces. Soil moisture creates pore pressure, which reduces the effective normal stress and shear strength. Pore pressure in the slope differs among sites and also has large temporal variation. It is difficult to estimate these values and to include them in this model of a large basin. Therefore, we simplified the condition of pore pressure in the slope by assuming that the pore pressure in the slope is always in the static state condition. Pore pressure is quantified by the following equation when assuming no excess pore water pressure:

$$u = \rho_w\, g\, h_w \cos\theta , \qquad (6)$$

where ρ_w is the density of water (= 1000 kg/m^3) and h_w is the height of the water depth perpendicular to the slope (m). This assumption gives greater pore water pressure in the rising process of the subsurface water and smaller pore water pressure in the descending process of the subsurface water.

The shear stress as driving force, defined by the downslope parallel component of gravity, can be expressed as follows:

$$\tau = \rho_s g \sin\theta\, d_a + W\sin\theta \qquad (7)$$

By substituting the formula for shear strength and shear stress, the factor of safety is calculated as follows

$$FS = \frac{c^* + \cos\theta\left[1 - r_w\right]\tan\phi}{\sin\theta}; \begin{cases} c^* = \dfrac{c_r + c_s}{d_a\rho_s g + W} \\[2mm] r_w = \dfrac{h_w\rho_w}{\left(1 + \dfrac{W}{gd_a\rho_s}\right)d_a\rho_s} \end{cases}$$

(8)

in which c^* is the total cohesion ($c_r + c_s$), c_r and c_s is the effective root and soil cohesion (N/m^2). The dimensionless form of Equation (6) has been widely used to analyse the stability of shallow soil using digital terrain models.

According to Equation (8), most of the variables could be set up as spatially distributed, but it is assumed that only h_w is time-varying. The water depth, h_w, is determined by the flux of subsurface water flow computed by the hydrological model (see Equation 1). Here the ratio ($m = h_w/d_a$) shows that the relative saturated depth is time-dependent (range numerically between 0.0 and 1.0). Whenever FS < 1.0, the driving forces prevail, and the potential for failure is high. Through an inversion of the standard factor of safety (Equation 8), a fixed time-invariant critical relative soil saturation (m^c) triggering slope instability (i.e., relative soil saturation that yields FS = 1.0) for each grid element could be approximated as

$$m^c = \left(\frac{\rho_s}{\rho_w} + \frac{W}{gd_a\rho_w}\right)\left(1 - \frac{\tan\theta}{\tan\phi}\right) + \frac{c_r + c_s}{d_a\rho_w g \cos\theta\tan\phi}$$

(9)

Based on the concept of critical relative soil saturation, three slope stability classes could be defined as theoretically "stable", potentially "stable/unstable", and theoretically "unstable" (Montgomery and Dietrich, 1994). The theoretically "**stable**" condition refers to those slopes that are stable even when saturated soil depth reaches the

ground surface, $m^c = 1.0$. Similarly, slopes that are predicted to be unstable even under a dry condition (i.e., $m = 0.0$) are considered to be theoretically "**unstable**"; such slopes affected by suction force or composed of rocks. In the unsaturated soil layer, suction (negative pore water pressure) is working and provides additional shear strength. This force is also difficult to include in the model at present. In addition, there is no subsurface flow processes for the slope elements where the soil mantle spaces composed by the impermeable bedrock. Therefore,

we excluded the slope areas characterized as theoretically "**unstable**" from the target of this research.

In this study, the critical relative soil saturation depth obtained by Equation (9) and time-dependent slope instability analysis were calculated only for those grids with slope stability classified as potentially "**stable/unstable**"; these grids were defined as the target area for simulating slope instability as a function of time.
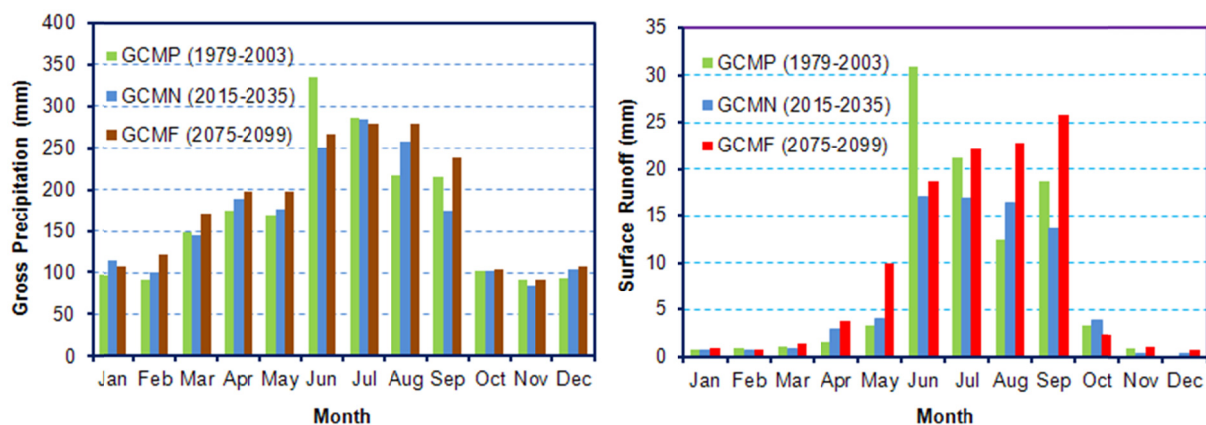

Fig. 2 Mean monthly gross precipitation (left chart) and surface runoff (right chart) in western Japan under three climate conditions: present climate (GCMP), near future climate (GCMN) and future climate (GCMF).

3. Simulation Results

Using the product of a very high-resolution atmospheric global climate model having 20-km spatial resolution (MRI-AGCM20) as the climate forcing data, the calibrated geohydrologic model was implemented with hourly output and 1-km grid resolution. The products of MRI-AGCM20 used in this study consist of the present climate (1979-2003), the near future climate (2015-2039) and the future climate condition (2075-2099). Area-weighted averaged precipitation component were calculated from the output AGCM20 (Figure 2). The Figure shows how the seasonal patterns are projected to be changed in the near future and future terms comparing to the present pattern. In the future climate condition, peak time and magnitude of gross precipitation in June and July decreases, while it is

going to be shifted to and increase in August. Changes in 2075-2099 yield a significant increase in August and September precipitation relative to the present climate. In addition, monthly precipitation and surface runoff in winter season will increase.

The geohydrological model parameters were adjusted using observed streamflow discharge, annual dam sedimentation, and landslide inventory in order to obtain optimal model performance in major river basins, including the Yoshino (Figure 3) and Chikugo. The same calibrated model parameters were used for all river basins across the region for 75 years simulations. Figures 4 & 5 show spatial patterns of the percent change of mean August hydrologic variables, soil detachment, and unstable slope probability in the future climate condition with respect to the present climate condition. The results suggest that the river basins hydrological responses to

precipitation changes under the future climate is going to have direct impact on soil productions and slope instability. The study found a 5-75% increase in August precipitation to be associated with up to an approximate 1% to 20% of change in streamflow discharge, 1% to 30% of increase in soil production and 1% to 50% of increase in shallow landslide probability. Hotspots of significant changes differ according to the time and location. Kochi, Tokushima, Miyazaki, Kumamoto, Hiroshima, Yamaguchi, Ehime, Shimane and Okajama Prefectures are expected to be hotspots. The following research is underway for further improvement and upgrading the simulation by utilizing MRI-RCM5km and bias-corrected MRI-GCM20, by simulating dam sedimentation and riverbed change and by conducting risk-based analysis as well as by designing feasible adaptation measures.
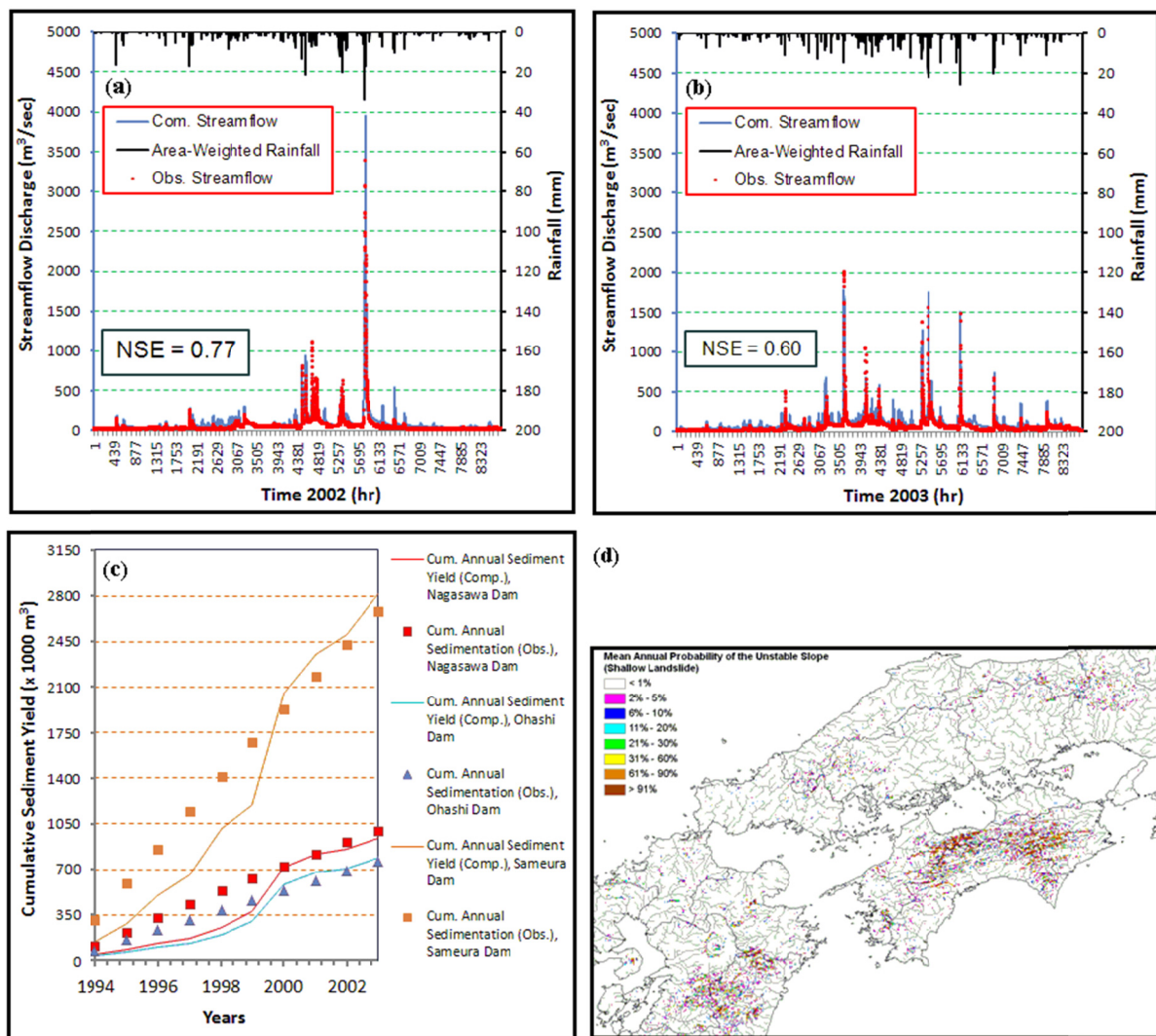

Fig. 3 Several results of model evaluation: (a) computed and observed hourly streamflow discharges during calibration period (2002) at Toyonaga station, Yoshino River basin; (b) computed and observed hourly streamflow discharges for validation period (2003) at Toyonaga station, Yoshino River basin; (c) comparison between computed and observed cumulative sediment yields for three dams in the Yoshino River basin; and (d) spatial distribution of estimated shallow landslide susceptibility map and its mean annual probability.
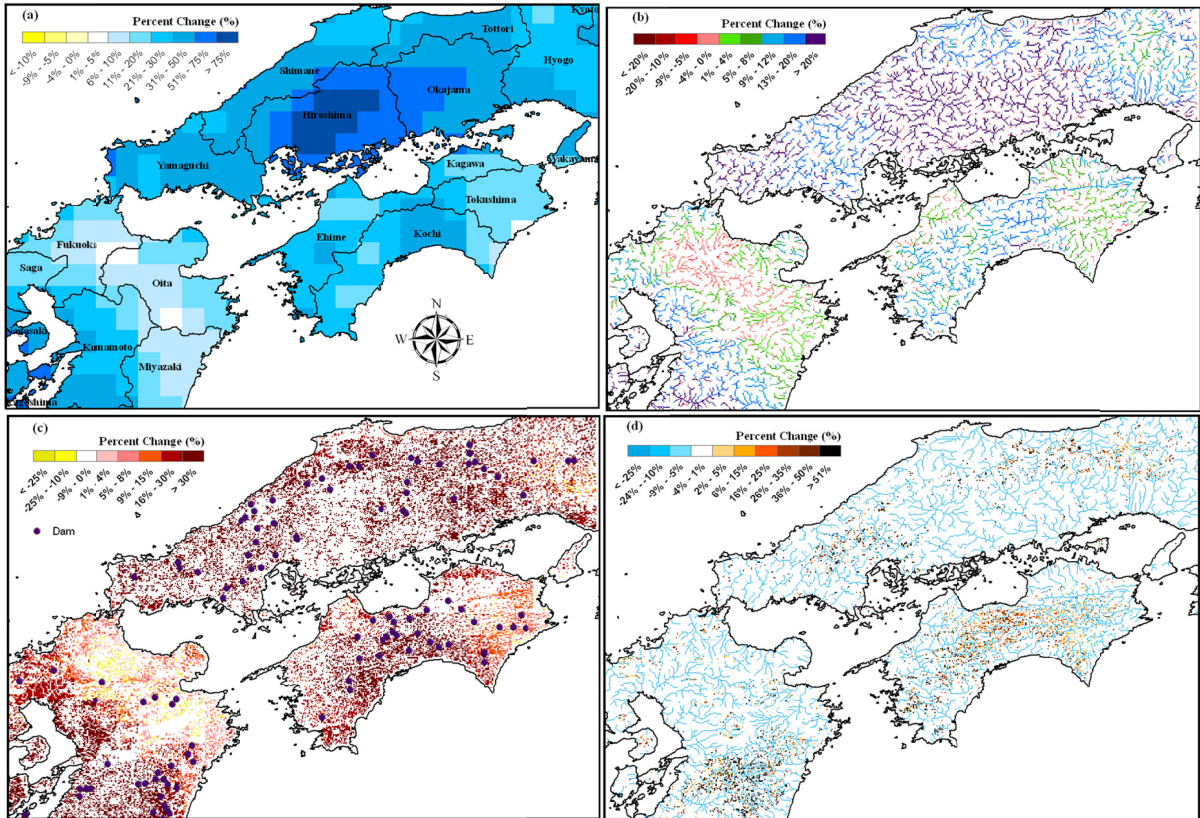
Fig. 4 Projected changes (percentage difference) of mean August (a) gross precipitation, (b) streamflow discharge, (c) soil detachment and (d) unstable slope (shallow landsliding) probability in the future climate condition with respect to the present climate condition.
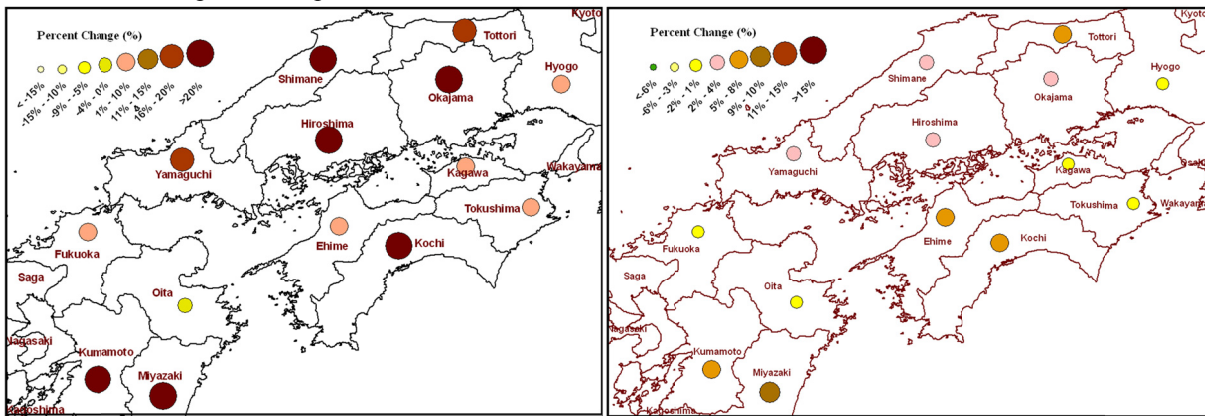

Fig. 5 Projected percent changes of the area-weighted mean August soil detachment (left chart) and shallow landslide probability (right chart) of each prefecture in the future climate with respect to the present climate.

4. Conclusions

In the future climate condition, peak time and magnitude of gross precipitation in June and July decreases, while it is going to be shifted to and increase in August. Changes in 2075-2099 yield a significant increase in August and September precipitation relative to the present climate. In addition, monthly precipitation and surface runoff in winter season will increase.

The results suggest that the river basins hydrological responses to precipitation changes under the future climate is going to have direct impact on soil productions and slope instability. The study found a 5-75% increase in August precipitation to be associated with up to an approximate 1% to 20% of change in streamflow discharge, 1% to 30% of increase in soil production and 1% to 50% of increase

55

in shallow landslide probability. Hotspots of significant changes differ according to the time and location. Kochi, Tokushima, Miyazaki, Kumamoto, Hiroshima, Yamaguchi, Ehime, Shimane and Okajama Prefectures are expected to be hotspots.

The following research is underway for further improvement and upgrading the simulation by utilizing MRI-RCM5km and bias-corrected MRI-GCM20, by simulating dam sedimentation and riverbed change and by conducting risk-based analysis as well as by designing feasible adaptation measures.

References

IPCC. (2007): Climate change 2007: the physical science basis. Contribution of working group I to the fourth assessment report of the Intergovernmental Panel on Climate Change. Cambridge University Press, Cambridge.

Foster, G.R. (1982): Modelling the erosion process. In: Hydrologic Modelling of Small Basins. American Society of Agricultural Engineers, St. Joseph, 295–380.

Ghosh, S., and Misra C. (2010): Assessing hydrological impacts of climate change: modeling techniques and challenges. The Open Hydrology Journal, Vol. 4, pp 115-121.

Kojima, T., and Takara, K. (2003): Grid-cell based distributed flood-runoff model and its performance, weather radar information and distributed hydrological modeling. IAHS Publications, Vol. 282, pp 234–240.

Montgomery, D.R., and Dietrich, W.E. (1994): A physically-based model for the topographic control on shallow landsliding. Water Resources Research, Vol. 30, pp. 1153-1171.

Sayama, T., and McDonnel, J.J. (2009): A new time-space accounting scheme to predict stream water residence time and hydrograph source components at the watershed scale. Water Resources Research, 45: pp. 1-14

Tachikawa, Y., Nagatani, G., and Takara, K. (2004): Development of stage-discharge relationship equation incorporating saturated-unsaturated flow mechanism. Annual Journal of Hydraulic Engineering (JSCE), pp 48: 7-12.

気候変動が西日本の土砂生産に与える潜在的影響評価

APIP・宝　馨・小林健一郎[1]・山敷庸亮・中北英一

[1]京都大学学際融合教育研究推進センター　極端気象適応社会教育ユニット

要　旨

本研究では気候変動が西日本の地域レベルでの土砂生産及び斜面不安定性に与える潜在的な影響をシミュレーションにより評価する。気象研究所の気候モデル（MRI-AGCM20）により計算された 20km 解像度の降雨データを地質水文モデルに入力し，時間解像度 1 時間，空間解像度 1km でこの影響評価を実施する。結果として，将来気候下での降雨変化が，河川流域における土砂生産と斜面不安定性に影響を及ぼすことがわかった。将来気候下では，6 月と 7 月の総降水量が減少するが，8 月の総降水量は増加する．西日本の各地域で 8 月に 5〜75%総降雨が増加し，これにより河川流量が 1〜20%増加，土砂生産は 1〜30%の増加，浅層崩壊は 1〜50%増加することわかった。特に変化が顕著な地域は時期と位置により異なる。

キーワード:地質水文モデル，気候変動，西日本，土壌侵食，土砂生産，浅層崩壊